Order-disorder behavior in the ferroelectric nematic phase investigated via Raman spectroscopy

Thomas Raistrick,[1,*] Richard J. Mandle,[1,2] Zhaopeng Zhang,[1] Peter J. Tipping,[1] and Helen F. Gleeson[1]
[1]*School of Physics and Astronomy, University of Leeds, Leeds LS2 9JT, United Kingdom*
[2]*School of Chemistry, University of Leeds, Leeds LS2 9JT, United Kingdom*

(Received 26 April 2024; accepted 22 August 2024; published 15 October 2024)

Polar-ordered fluids are of interest both fundamentally and from an application standpoint. The recently discovered ferroelectric nematic phase is an example of a polar-ordered fluid, and while there has been extensive research interest in these materials, some of the fundamental properties are yet to be fully understood. Here, we report the order parameters of one of the first known materials that exhibit a ferroelectric nematic phase, RM734, determined via Raman spectroscopy. Raman spectroscopy been used extensively to determined order parameters in liquid crystals systems but also to probe ferroelectric behavior in solid ferroelectric systems and is therefore a powerful technique to study the ferroelectric nematic phase. A reduction and subsequent recovery of order parameters ($\Delta\langle P_2\rangle \approx 0.1$, $\Delta\langle P_4\rangle \approx 0.06$) is observed near the onset of the **N** to $\mathbf{N_F}$ transition, a feature that is confirmed via complementary birefringence measurements. This dip in order parameters has been attributed to splay fluctuations, which occur at the onset of the $\mathbf{N_F}$ transition; here we suggest a different explanation. A broadening of the full-width half-maxima (FWHM), of the order of 1 cm^{-1}, of the selected Raman peak is observed near the **N** to $\mathbf{N_F}$ phase transition, which we relate to either a change in reorientational dynamics or the onset of polar order. The $\mathbf{N_F}$ transition is analyzed using standard solid ferroelectric frameworks. An energetic barrier associated with the para- to ferroelectric transition is found to be of the order of 2.5 ± 0.6 kJ/mol, which is comparable to solid ferroelectric materials.

DOI: 10.1103/PhysRevE.110.044702

I. INTRODUCTION

Almost a century after its theoretical prediction [1], the ferroelectric nematic ($\mathbf{N_F}$) liquid crystal phase was experimentally realized in 2017 [2–4]. The fundamental interest in the $\mathbf{N_F}$ phase as a polar, ordered fluid system is enhanced by the fact that these materials are reported to have exceptionally large dielectric permittivities [4,5] and spontaneous polarization values [4,6]. As such, $\mathbf{N_F}$ materials are expected to have far-reaching implications in applications such as nonlinear optical devices [7], fluid capacitors for energy storage [4], and photonic devices [8].

The conventional nematic (**N**) phase is apolar, meaning that there is inversion symmetry of the director ($\hat{\mathbf{n}}$), which describes the average direction of orientational order, such that $\hat{\mathbf{n}} = -\hat{\mathbf{n}}$. Consequently, the apolar **N** phase can be described using only even terms of order parameters, $\langle P_n\rangle$, where P_n is the nth order Legendre polynomial function [9]. Conversely, the $\mathbf{N_F}$ phase has polar ordering, and due to the ordered polarization of the molecular dipoles, the inversion symmetry of the phase is broken such that $\hat{\mathbf{n}} \neq -\hat{\mathbf{n}}$ [10]. Thus, in the $\mathbf{N_F}$ phase, odd terms of order parameters (e.g. $\langle P_1\rangle$, $\langle P_3\rangle$) become relevant. Schematics of these phases are shown in Fig. 1. The macroscopic properties of a bulk liquid crystal phase are often related to the physical properties of the molecules themselves, their interactions with each other, and the state of the ordering in the system. Given the remarkable properties of the ferroelectric nematic phase and its far-reaching applications, it is of utmost importance to understand the state of order within the phase.

The order in the $\mathbf{N_F}$ phase has been investigated experimentally via x-ray scattering [11], and through theoretical [12,13] and molecular dynamic frameworks [14]. Raman spectroscopy has been used extensively to study the order parameters in the apolar nematic phase [15–17], however, it is yet to be used in understanding the behavior of the ferroelectric nematic phase. In fact, Raman spectroscopy is particularly useful in this regard when compared to other techniques for three primary reasons: (i) Raman spectroscopy allows one to determine not only the low-rank uniaxial order parameter $\langle P_2\rangle$ but the higher-order $\langle P_4\rangle$ term, along with the second and fourth rank biaxial order parameters [18,19], providing a detailed description of the state of order in liquid crystal phases; (ii) Raman spectroscopy can probe physical properties of ferroelectric nematics without the application of an external field, which may cause screening or flexoelectric effects that might affect some measurements [20]; (iii) in addition to its use in studying liquid crystal phases, Raman spectroscopy has been used extensively to study the paraelectric to ferroelectric transition in ferroelectric solids such as ferroelectric polymers [21], ferroelectric ceramics [22], ferroelectric metals [23], and molecular ferroelectrics [24]. Thus, the study of the ferroelec-

*Contact author: t.j.raistrick@leeds.ac.uk

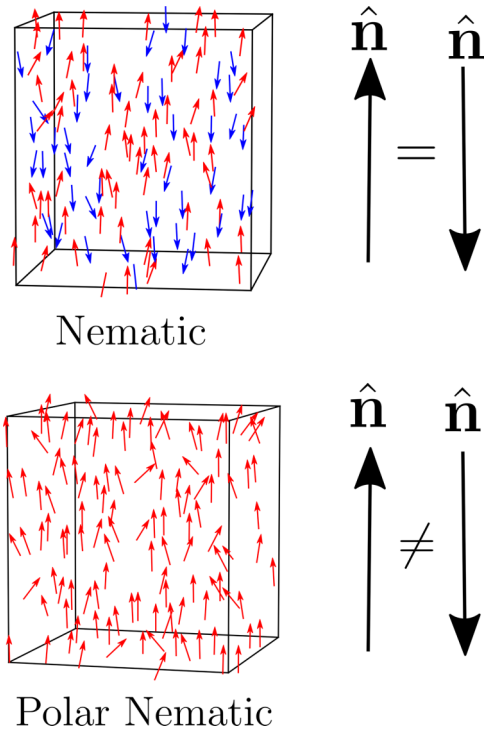

FIG. 1. Schematic of the (apolar) nematic, **N**, phase and the polar nematic phase, $\mathbf{N_F}$. The arrows denote the dipoles of each molecule.

tric nematic phase via Raman spectroscopy, as is reported here, allows one to compare the behavior within the phase to both the apolar nematic phase and conventional (solid) ferroelectric materials using a single technique. In this paper, we use Raman spectroscopy to investigate both aspects of the physics of the $\mathbf{N_F}$ phase.

So far, there are relatively few measurements of order in ferroelectric nematic liquid crystals. Small- and wide-angle x-ray scattering measurements (SAXS and WAXS, respectively) on one of the first-reported compounds exhibiting an $\mathbf{N_F}$ phase, RM734 (Fig. 2), determined the value of the uniaxial, nonpolar order parameters up to the tenth order ($\langle P_n \rangle$, $n = 2, \ldots, 10$) [11]. Only the terms from $\langle P_2 \rangle$ to $\langle P_6 \rangle$

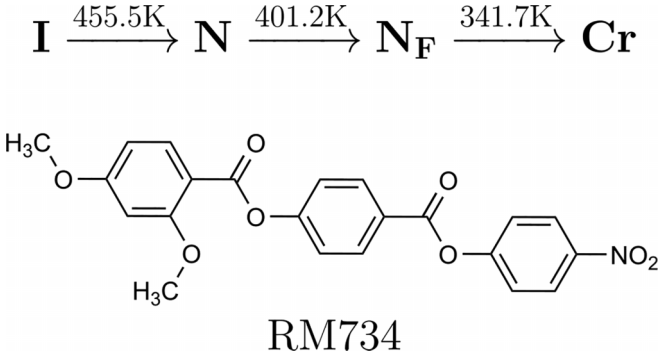

FIG. 2. Chemical structure of RM734 and phase transition temperatures as determined via differential scanning calorimetry (DSC) on cooling at a rate of 10 K/min. The notation of the phases is as follows: **I**, isotropic; **N**, nematic; $\mathbf{N_F}$, ferroelectric nematic; **Cr**, crystal.

were found to be nonzero in the **N** phase and a small increase in their values was observed at the **N** to $\mathbf{N_F}$ transition. The birefringence of a liquid crystal can be considered to be a proxy for the $\langle P_2 \rangle$ order parameter [17] and a similar increase in the birefringence of RM734 as it was cooled into the $\mathbf{N_F}$ phase, suggesting an increase in order, was reported by Chen *et al.* [6]. Due to surface anchoring effects, the type of alignment used can have significant effects on the textural evolution of ferroelectric nematic liquid crystals [25], therefore, a detailed comparison of the birefringence data for RM734 from the literature is complicated due to the various cell geometries and alignment techniques used within the studies. For example, recently Barthakur *et al.* [26] reported birefringence measurements on RM734 that show a marked reduction in the birefringence, just before the **N** to $\mathbf{N_F}$ transition, which is not observed in the reports of Mandle *et al.* [11] and Chen *et al.* [6]. The reduction in birefringence observed by Barthakur *et al.*, performed in antiparallel cells, was related to critical pretransitional splay fluctuation effects [26,27]. Interestingly, birefringence measurements on an RM734 homologue, also in an antiparallel planar cell, produced no such reduction in birefringence before the transition to the $\mathbf{N_F}$ phase [28], which suggests that observation of a reduction in birefringence is not necessarily related to alignment and the phenomenon is worthy of further investigation. The nature of the evolution of order from the **N** to $\mathbf{N_F}$ phase needs to be fully understood in order to help to determine the physics behind the ferroelectric nematic phase formation in general.

In this paper, we report the uniaxial order parameters ($\langle P_2 \rangle$, $\langle P_4 \rangle$) of RM734 as determined via Raman spectroscopy in parallel planar aligned cells. The data are considered alongside birefringence measurements on a device with the same alignment conditions but different thickness. Our results are compared and contrasted to the order parameters determined via x-ray scattering reported by others [11]. We discuss our findings by drawing parallels between the ferroelectric nematic fluid phase and solid ferroelectric materials as investigated via Raman spectroscopy. It is suggested that the existence of polar order, and/or a change in the reorientational dynamics of the molecules, at the onset of the $\mathbf{N_F}$ phase may be reflected in the full-width half-maxima (FWHM, Γ) of the Raman signal.

II. METHODS

RM734 (chemical structure shown in Fig. 2) was synthesized as described previously [3]. The phase transitions of RM734 were confirmed via both polarized microscopy and differential scanning calorimetry (DSC), the latter using the TA Instruments Q2000 on cooling at a rate of 10 K/min. To perform the optical birefringence and Raman spectroscopy measurements, RM734 is filled into liquid crystal cells comprising two parallel plates of glass with a predefined cell gap. The glass plates are treated with rubbed SE130 polyimide alignment layers and constructed so as to achieve homogeneous parallel planar alignment (AWAT, Poland).

Uniaxial order parameters are deduced via Raman spectroscopy as described in detail previously [15,16] and briefly summarized as follows. The aligned liquid crystal sample, with a thickness of 20 μm is placed in a Linkam hot stage to

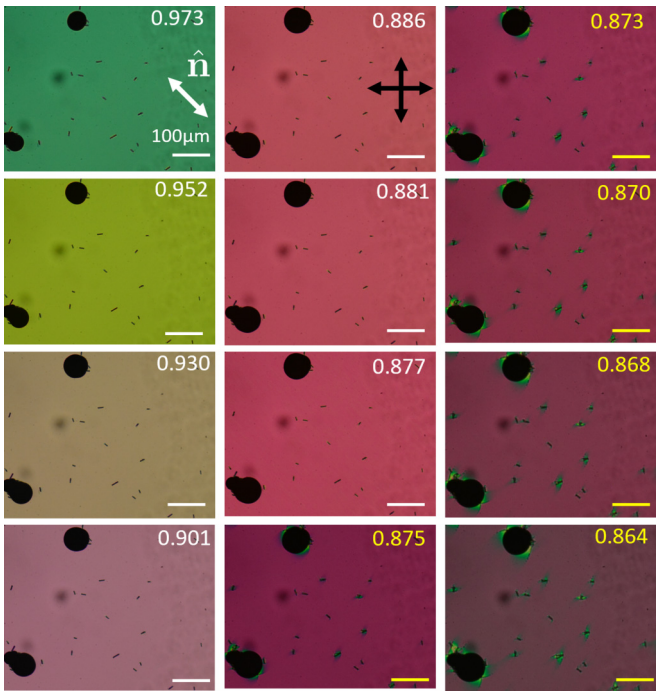

FIG. 3. Optical texture of RM734 in a 5 μm parallel planar rubbed cell confirming homogeneous optical textures in both the **N** (white) and $\mathbf{N_F}$ phases (yellow). The white arrows indicates the rubbing direction and the black arrows indicate the analyser and polarizer orientation.

allow for temperature control (relative accuracy ±0.1 K). The hot stage, with the sample, is placed in the Renishaw inVia Raman spectrometer, which includes an optical microscope with a rotation stage. A 50× microscope objective is focused on the top of the sample. The liquid crystal sample is illuminated with a 20 mW 532 nm laser (spot size ∼5 μm) and an exposure of 30 s selected; the backscattered Raman spectra are recorded via a CCD. The power and exposure time of the incident laser power are selected to achieve optimal signal-to-noise ratio while avoiding overexposure, which can lead to sample aging. The Raman spectra are recorded for parallel and perpendicular scattering configurations and for orientations of the nematic director at 10° intervals from 0°–360° with respect to the incident laser polarization. Measurements were taken in well-aligned regions of the sample away from any domain boundaries. Polarized optical microscopy images of RM734 are shown in Fig. 3 confirming homogeneous optical textures in the **N** and $\mathbf{N_F}$ phases.

Order parameters are determined using the phenyl C-C stretching mode (∼1606 cm^{-1}) as it most closely satisfies the assumptions required for order parameter calculations via Raman spectroscopy [16]; namely that the (i) selected vibration mode is cylindrically symmetric and (ii) selected vibration is along the long axis of the molecule. The intensity of the Raman peak for each configuration is deduced by fitting the line associated with the phenyl C-C stretching mode with a Lorentz function. The ratio of the perpendicular to parallel intensity, the depolarization ratio, $R(\theta)$, is thus deduced as a function of the angle of the nematic director of the sample with respect to the incident laser polarization (θ). Order parameters are deduced by fitting to $R(\theta)$ using equations 1 and 2 for the intensity of the scattered light parallel, $I_\parallel$, and perpendicular, $I_\perp$ to the incident laser polarization.

$$I_\parallel(\theta) \propto \frac{1}{5} + \frac{4r}{15} + \frac{8r^2}{15}\rangle + \langle P_2\rangle\left[\frac{1}{21}(3 + r - 4r^2)[1 + 3\cos(2\theta)]\right] + \langle P_4\rangle\left[\frac{1}{280}(1-r)^2[9 + 20\cos(2\theta) + 35\cos(4\theta)]\right], \quad (1)$$

$$I_\perp(\theta) \propto \frac{1}{15}(1-r)^2 + \langle P_2\rangle\left[\frac{1}{21}(1-r)^2\right] + \langle P_4\rangle\left[\frac{1}{280}(1-r)^2[3 - 35\cos(4\theta)]\right]. \quad (2)$$

In these equations, r is the differential polarizability ratio relating to the differential polarizability tensor, θ is the angle of the sample director with respect to the laser polarization, $\langle P_2\rangle$ and $\langle P_4\rangle$ are, respectively, the second and fourth rank uniaxial order parameters, which are given by Eqs. (3) and (4),

$$\langle P_2\rangle = \tfrac{1}{2}\langle 3\cos^2(\beta) - 1\rangle, \quad (3)$$

$$\langle P_4\rangle = \tfrac{1}{8}\langle 3 - 30\cos^2(\beta) + 35\cos^4(\beta)\rangle, \quad (4)$$

where $\langle\rangle$ denotes an ensemble average and β is the angle between the molecular long axis and the nematic director $\hat{n}$.

The birefringence of RM734 is determined via a Berek compensator and polarizing optical microscopy. The cell gap of the LC is determined with an accuracy of ±0.1 μm prior to filling via the reflection spectra measured using a UV-vis spectrometer and a white light source. Cell thicknesses of ∼5 μm were used to reduce the issues related to dispersion mismatch between the sample and Berek compensator [29,30]. An aligned liquid crystal sample is placed in a Linkam hostage to allow for temperature control (relative accuracy ±0.1 K). The hot stage is housed in a polarizing microscope equipped with a Berek compensator. A white light source filtered to provide a wavelength of 589 nm is used. The retardance of the sample is measured and the birefringence of the sample is calculated with an accuracy of ∼4% by dividing the retardance by the sample thickness.

III. RESULTS

The uniaxial order parameters, $\langle P_2\rangle$ and $\langle P_4\rangle$ of RM734 as determined via Raman spectroscopy are shown in Fig. 4 as a function of reduced temperature (T/T_{NI} where T_{NI} is the nematic to isotropic transition temperature). Within the nematic phase, values of $\langle P_2\rangle$ and $\langle P_4\rangle$ are nonzero and upon further cooling in the nematic phase $\langle P_2\rangle$ and $\langle P_4\rangle$ are found to increase, with maximum values of $\langle P_2\rangle = 0.67 \pm 0.05$ and $\langle P_4\rangle = 0.26 \pm 0.05$ observed at $T/T_{NI} \approx 0.908$. Interestingly, upon cooling further approaching the **N** to $\mathbf{N_F}$ transition, a decrease in both $\langle P_2\rangle$ and $\langle P_4\rangle$ is observed and a local

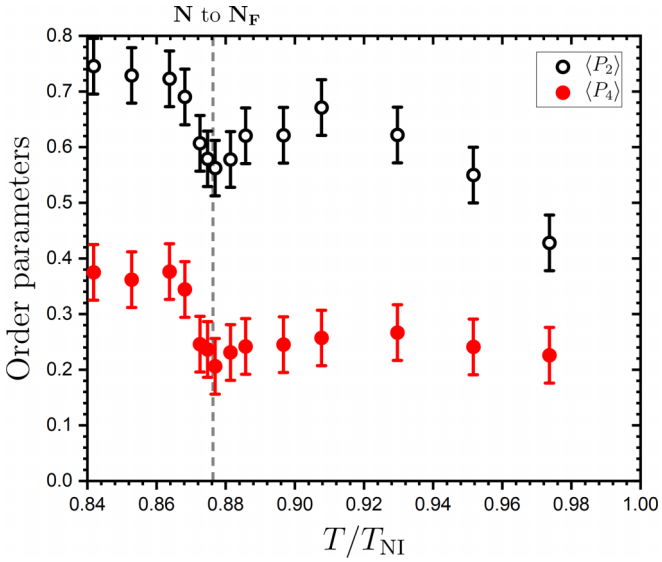

FIG. 4. Uniaxial order parameters $\langle P_2 \rangle$ (hollow circles) and $\langle P_4 \rangle$ (filled circles) as a function of reduced temperature for RM734 determined from the phenyl C-C stretching mode as determined via Raman spectroscopy. The vertical dashed line indicates the **N** to $\mathbf{N_F}$ phase transition.

minimum in $\langle P_2 \rangle$ and $\langle P_4 \rangle$ is seen close to the **N** to $\mathbf{N_F}$ transition. Cooling further into the $\mathbf{N_F}$ phase, both uniaxial order parameters are observed to increase monotonically. The dip in the magnitude of order parameters in the **N** phase before the phase transition is surprising and has not been reported for other liquid crystal phase transitions. This unusual temperature dependence of the order parameters can be explored further by comparing the data with completely independent measurements, i.e., the birefringence of RM734. Figure 5 shows the $\langle P_2 \rangle$ data plotted together with the birefringence (Δn) as a function of reduced temperature. The birefringence takes values between ∼0.1 and ∼0.3 across

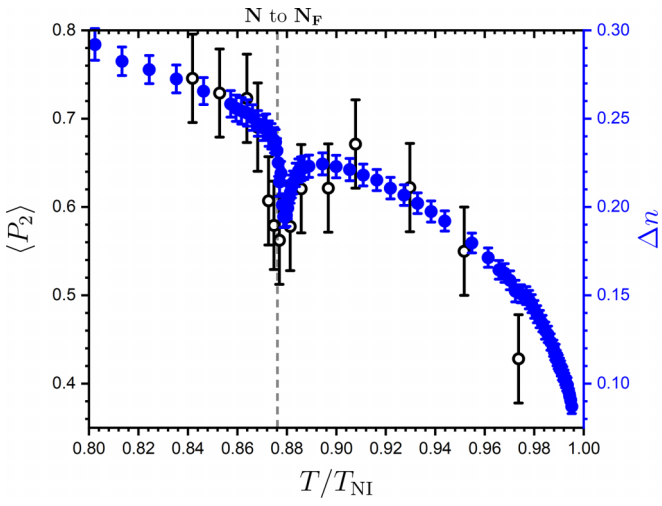

FIG. 5. The order parameter, $\langle P_2 \rangle$ (hollow circles), and birefringence (filled circles), Δn, of RM734 as a function of reduced temperature. The vertical dotted line indicates the **N** to $\mathbf{N_F}$ phase transition.

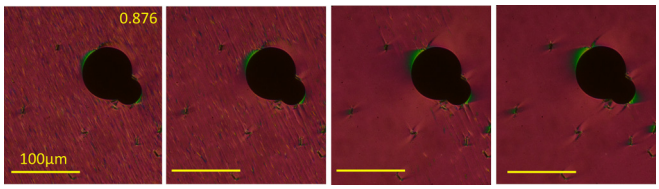

FIG. 6. Stripe textures forming just above the **N** to $\mathbf{N_F}$ transition. The stripe textures stabilise leading to homogeneous alignment of the $\mathbf{N_F}$ phase after clearing.

the temperature range, with a dip of ∼0.03 just above the **N** to $\mathbf{N_F}$ phase transition. Figure 5 demonstrates that there is a strong correspondence between $\langle P_2 \rangle$ and Δn in both the **N** and $\mathbf{N_F}$ phase of RM734, as expected [17]. Interestingly, the pretransitional reduction in both parameters is observed on the approach to the **N** to $\mathbf{N_F}$ transition temperature.

It should be noted that just above the **N** to $\mathbf{N_F}$ transition domain instability is observed as shown in Fig. 6. This domain instability has been previously reported in RM734 [10,27]. Care was taken to ensure measurements were performed sufficiently far away from any striped textures, in homogeneously aligned regions within the cell. Given that the reduction in order parameters and Δn is observed ∼7 K above the transition the reduction cannot be attributed to the domain instability observed at the transition and, as discussed later in the text, is likely capturing pretransitional behavior.

It is interesting to compare the order parameters reported in this work with those determined from x-ray scattering, and to consider both in the context of Maier-Saupe theory [31,32]. We first consider the Raman and x-ray data. Figure 7(a) shows the $\langle P_2 \rangle$ and $\langle P_4 \rangle$ data determined via Raman spectroscopy together with data determined via x-ray taken from [11]. There is reasonable agreement of the $\langle P_2 \rangle$ data from both techniques, though there is no indication of the pretransitional dip from the x-ray data. The Raman data return consistently higher-order parameters, particularly in the $\mathbf{N_F}$ phase and in particular, the $\langle P_4 \rangle$ order parameter deduced from Raman scattering is consistently higher than that determined from x-ray scattering.

Both data sets can also be compared with Maier-Saupe theory, which describes the evolution of $\langle P_2 \rangle$ as a function of T by considering a simple mean-field approach of an anisotropic pair potential. Maier-Saupe theory considers long-range attractive forces and predicts the nematic to isotropic transition in liquid crystals along with the magnitude and evolution of $\langle P_2 \rangle(T)$ with reasonable success [32]. Here, we have extended the theoretical prediction continuously into the $\mathbf{N_F}$ phase. Again, it can be seen from Fig. 7(a) that there is reasonable agreement between the theory and $\langle P_2 \rangle$ deduced from both techniques. However, the dip seen for the Raman data at the **N** to $\mathbf{N_F}$ transition is not predicted. Additionally, the agreement of $\langle P_2 \rangle$ from the x-ray data becomes worse as the temperature is reduced further away from T_{NI}.

Additional insight into the agreement (or otherwise) of the experimental data with the mean-field Maier-Saupe theory can be gained by plotting $\langle P_4 \rangle$ against $\langle P_2 \rangle$. Figure 7(b) shows order parameter data plotted this way, allowing one to examine the temperature-independent relationship between the two

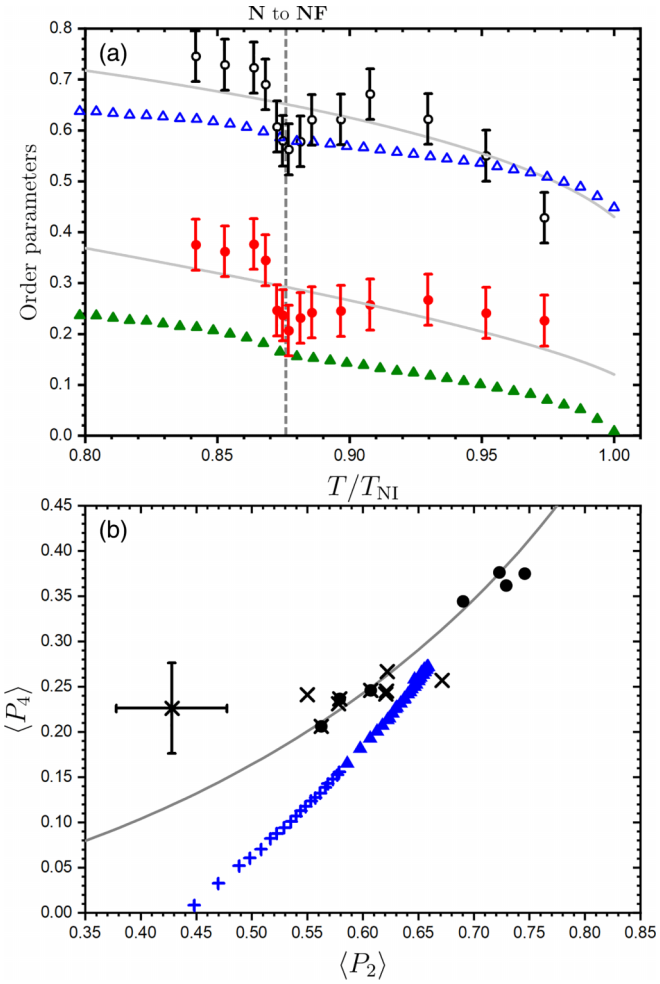

FIG. 7. The order parameters $\langle P_2 \rangle$ and $\langle P_4 \rangle$ determined via Raman (black hollow and red filled circles, respectively) and x-ray scattering (blue hollow and green filled triangles, respectively) compared to Maier-Saupe mean-field theory (gray solid line) on a reduced temperature scale. The vertical dashed line indicates the **N** to $\mathbf{N_F}$ phase transition. (b) $\langle P_4 \rangle$ is plotted as a function of $\langle P_2 \rangle$, the data points from the Raman experiment within the nematic phase are shown as black diagonal crosses whereas the ferroelectric nematic phase data are shown in filled black circles; experimental error is shown on one data point for clarity. X-ray order parameter data (from [11]) within the nematic phase are shown as blue upright crosses whereas the ferroelectric nematic phase data are shown as blue filled triangles. The gray line represents $\langle P_4 \rangle$ predictions for a given $\langle P_2 \rangle$ from Maier-Saupe theory. In both (a) and (b) the x-ray data are taken from Ref. [11].

order parameters. The measurements from Raman spectroscopy in both the nematic and ferroelectric nematic [Fig. 7(b), crosses and filled circles, respectively] are in excellent agreement with the mean-field Maier-Saupe theory. However, the agreement of the x-ray data, taken from Ref. [11], with theory is not particularly good. Indeed, the deviation of the order parameters determined from x-ray data when compared to Maier-Saupe theory was discussed in Ref. [11] where it was argued that the deviation may be due to Maier-Saupe theory being developed for apolar uniaxial nematic phases. However, given the similarity of the order parameters determined from the Raman data to Maier-Saupe theory, and the disagreement with the order parameters even in the apolar nematic phase of RM734 as determined via x ray, the deviation may alternatively be related to how order parameters are constructed from x-ray data; this point will be discussed in further detail in the next section. Much theoretical work on the $\mathbf{N_F}$ phase is based upon expanding Maier-Saupe theory [12,13], in the case of generalized mean-field theory, or Lebwohl-Lasher pair potentials [33], in the case of Monte Carlo simulations, to include a polar term. Such approaches appear to be validated by the results from Raman spectroscopy by considering the evolution of $\langle P_2 \rangle(T)$ and $\langle P_4 \rangle(T)$ [Fig. 7(a)] with respect to Maier-Saupe predictions within the **N** phase, though they do not capture the anomalous pretransitional dip seen in the order of the system determined through optical measurements.

IV. DISCUSSION

There are two key aspects of the results to discuss. First, the order parameters as measured by Raman scattering, when compared to published data deduced from x-ray scattering. There are numerous papers that compare order parameters that have been determined using both techniques, including in conventional nematic [34,35], twist-bend nematic [36], and ferroelectric smectic [37] liquid crystal phases. The order parameter values determined via x ray are found to be consistently smaller than those determined via Raman [34–37]. The difference in the determined order parameters is generally greater for $\langle P_4 \rangle$ than $\langle P_2 \rangle$ and our results are in line with all of these findings.

We consider now the birefringence data. In this work we report a birefringence value of $\Delta n = 0.225 \pm 0.007$ close to the **N** to $\mathbf{N_F}$ phase transition, with a pretransitional reduction in Δn of 0.030 ± 0.009 seen just above the transition. Recall that the measurements were taken at 589 nm, on monodomain regions void of defect boundaries in a device of ∼5 μm thickness with parallel planar alignment. Pretransitional behavior similar to that found herein has been described previously by a few authors. Mertelj *et al.* reported the birefringence of RM734 over a range from ∼5 K below the **N** to $\mathbf{N_F}$ transition and ∼15 K above it, though not immediately below the transition (∼0.5–2 K) [27]. All of their data for Δn differ in magnitude from that shown in Fig. 5, with $0.18 \lesssim \Delta n \lesssim 0.20$ over the temperature range studied and a dip in Δn of magnitude ∼0.05. Further, the temperature dependence is quite different, most notably with decreasing Δn from around 2 K above the **N** to $\mathbf{N_F}$ phase transition, behavior which is attributed to splay fluctuations. Barthakur *et al.* also reported Δn for RM734 as a function of temperature, with values much closer to those reported here (values were $0.05 \lesssim \Delta n \lesssim 0.22$ with the lowest temperature still quite close to the **N** to $\mathbf{N_F}$ phase transition). They also saw a dip of magnitude ∼0.01 close to the onset of the **N** to $\mathbf{N_F}$ transition, which they attributed to coexistence of polar and nonpolar domains and defects at the transition [26].

It is worth considering whether other explanations could explain the pretransitional dip seen in the birefringence (and Raman-deduced order parameter) measurements. The elastic constants of nematic liquid crystals typically follow an S^2

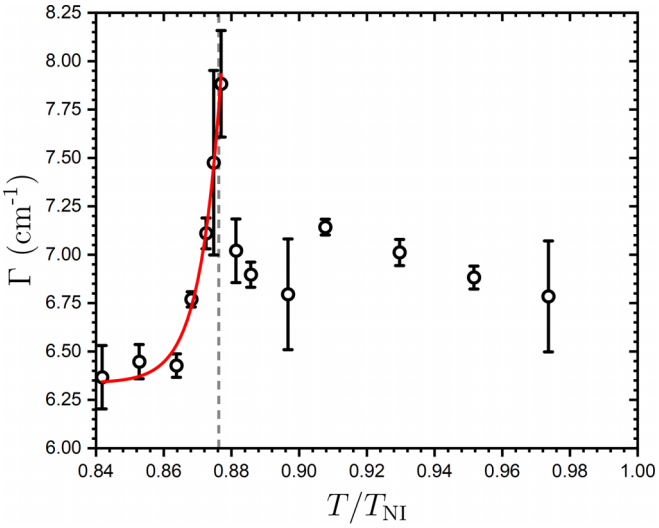

FIG. 8. Full-width half-maxima (FWHM), Γ, of the Lorentzian fit to the phenyl stretching mode, the solid red line is a fit to Eq. (7). The vertical dashed line indicates the **N** to $\mathbf{N_F}$ phase transition.

dependence [38] and while this may deviate significantly for noncalamitic (i.e., bent-core) liquid crystals, K_{ii} and S are still positively correlated [39,40]. In RM734, Mertelj *et al.* reported that on the approach to the $\mathbf{N_F}$ phase, there is a marked decrease in the splay and twist elastic constants [particularly the splay elastic constant (K_{11})] [27]. Therefore, the reduction of order parameters, as confirmed by Raman spectroscopy and birefringence measurements may reflect the pretransitional reduction of the splay elastic constant on the approach to the $\mathbf{N_F}$ phase. This reduction in K_{11} results in splay nematic director fluctuations, which in turn reduces birefringence [26]. Such director fluctuations could explain the reduction in the $\langle P_2 \rangle$ and $\langle P_4 \rangle$ value as determined via Raman spectroscopy [41,42], though it is puzzling that they were not captured in measurements using x-ray scattering.

However, one may additionally expect that strong short-range correlations are present in the ferroelectric phase and that these also change dramatically around the transition. Indeed, in RM734 evidence of increasing collective motion on cooling from the nematic to ferroelectric nematic phase, determined via dielectric spectroscopy, has been reported [7,43]. Interestingly, Raman spectroscopy can give also a direct insight into such phenomena from analysis of the line width. Specifically, it can give information on (i) reorientational dynamics and (ii) how $\mathbf{N_F}$ materials fit into a conventional ferroelectric framework.

Figure 8 shows the average FWHM, Γ, of the Lorentzian fits of the C-C phenyl stretching mode at $\theta = 0^\circ$ and 180° for parallel polarization. The FWHM at $T/T_{NI} \approx 0.973$ is 6.8 ± 0.3 cm^{-1}. Throughout the nematic phase, Γ varies only very slightly, taking values between 6.80–7.14 cm^{-1}. A sudden increase in Γ from 7.0 ± 0.2 cm^{-1} to 7.9 ± 0.3 cm^{-1} is observed on cooling from $T/T_{NI} \approx 0.881$–0.877 (a difference of 2 K), which is within 0.5 K of the **N** to $\mathbf{N_F}$ transition.

In-depth analysis of the changes in the Raman spectra line width allows one to separate contributions to the Raman signal that are vibrational from those that are rotational [44,45] and thus probe the reorientational time-scales of tumbling (rotation around the long axis) and spinning (rotation around the short axis) motions. The contribution of rotational dynamics to the Raman signal is complex and such analysis requires assumptions to simplify the analysis; these relate to the uniaxiality and rigidity of the molecule, the assignment of molecular rotation to a particular model [45], and the requirement of simple and isolated peaks in the Raman spectra such that Fourier transforms can be performed [44,46]. A complete analysis is therefore not attempted here. However, the implication of the FWHM broadening related to changes in reorientational dynamics is discussed; this is reasonable as:

(i) There is no significant change in the observed FWHM values in Fig. 8 throughout the **N** phase and Γ is comparable to values determined for mesogenic materials where a typical Γ of the order of 10 cm^{-1} is observed within nematic and smectic phases [45–48].

(ii) The change in the FWHM, $\Delta\Gamma \sim 1$ cm^{-1}, close to the **N** to $\mathbf{N_F}$ transition temperatures is comparable to broadening due to changes in rotational dynamics observed at phase transitions in mesogenic materials studied previously for example, $\Delta\Gamma \sim 0.2$–0.5 cm^{-1} is observed throughout the nematic phase due to changes in rotational dynamics and a change of $\Delta\Gamma \sim 2$ cm^{-1} is observed at the crystal to smectic A and smectic I to smectic C transition [45–48].

(iii) Very obvious director fluctuations, indicative of a change in dynamics, were observed herein via polarized microscopy on the approach to the $\mathbf{N_F}$ phase and have also been reported previously [26].

With the above in mind, we suggest that the clear change in Γ close to the **N** to $\mathbf{N_F}$ transition from $\Gamma \sim 6.75$ cm^{-1} to $\Gamma \sim 7.88$ cm^{-1} represents changes in the reorientational dynamics in RM734. An increase in FWHM is generally associated with an increase in rotational motion [44,49] with our data suggesting an abrupt increase close to the transition from the **N** to $\mathbf{N_F}$ phase, followed by a rapid decay within the $\mathbf{N_F}$ phase to values slightly lower than in the **N** phase ($\Gamma \sim 6.37$ at $T/T_{NI} \approx 0.841$). This may be related to findings via dielectric spectroscopy, whereby the molecular relaxation related to the flip flopping of molecules, or fluctuations of the polarization vector, become collective at the transition to the ferroelectric nematic phase and a softening is observed [7,43,50].

As discussed in the introduction, Raman spectroscopy has been used extensively to study the paraelectric to ferroelectric transition in solids [21–24]. It is often useful to study Raman hard modes (i.e., Raman peaks that are present above and below the Curie temperature, T_C) due to limitations with Raman soft modes in this regard [22,51]. Changes in the Raman signal in solid ferroelectrics have been observed at the paraelectric-ferroelectric transition in both the displacive and order-disorder type structural phase transitions [22,52]. In the context of ferroelectric solids, a displacive structural phase transition is one that is driven by ionic or atomic displacement often resulting in a change in the interatomic distance and symmetry of the unit cell [53]. The transition between the two phases is often associated with a phonon soft mode, which freezes throughout the transition [53,54]. In the context of ferroelectric solids, the order-disorder type transition is one in which above T_C the local polarization of the unit

cells persists, though there is no long-range ordering thus the net-polarization is zero [54]. It is important to note that displacive and order-disorder transitions are extreme cases of the ferroelectric phase formation and many materials fall somewhere between the two extrema [54,55]. With the above distinctions outlined, it is interesting to investigate the behavior of RM734 via Raman spectroscopy using the framework established for conventional ferroelectrics.

While the origin of how polar order develops in ferroelectric nematic phase is still a topic of much debate [10,14], and, as mentioned above, few materials fall into one of the extremes, and when compared to solid-state ferroelectric materials, the $\mathbf{N_F}$ phase behavior is closest to that seen in order-disorder type ferroelectrics. In solid-state order-disorder type ferroelectric materials, a peak in the FWHM of selected Raman signals has been observed at the transition from paraelectric to ferroelectric phases [24,56,57]. The broadening of Raman peaks is related to the self-diffusive fluctuation of the mode associated with the orientational order parameter [57,58]. The self-diffusive process is associated with a time scale, τ_{R}, relating to the probability of a particle or molecule jumping from one position to another (or from one energetic potential to another) with an activation energy, ΔU [57,58]:

$$\tau_R = \tau_0 \exp\left(\frac{\Delta U}{k_{\mathrm{b}} T}\right), \tag{5}$$

where k_{b} is the Boltzmann constant, and T is temperature. The temperature dependence of the FWHM broadening associated with this self-diffusion follows a Langevin function [57]:

$$\Gamma = [a + bT] + \left(c \frac{\tau_R}{1 + (2\pi\nu)^2 \tau_R^2}\right), \tag{6}$$

where a and b are fitting parameters and $[a + bT]$ is the anharmonic component of the Raman signal, ν is the wave number of Raman mode. Given that $(2\pi\nu)^2\tau_R^2 \gg 1$, Eq. (6) can be written in terms of the activation energy, ΔU:

$$\Gamma = [a + bT] + c \times \exp\left(\frac{-\Delta U(T)}{k_{\mathrm{b}} T}\right). \tag{7}$$

The FWHM, Γ, of the C-C phenyl stretching mode of RM734 can be analyzed using the framework developed for solid disorder-order type ferroelectrics. Fitting Γ below T_{C} (taken to be the $\mathbf{N}$ to $\mathbf{N_F}$ transition temperature) results in $\Delta U = 2.5 \pm 0.6\,\mathrm{kJ/mol}$. The energy scale of the disorder-order type transition leading to ferroelectricity in RM734 is considerably lower (albeit same order of magnitude) than those reported in solid ferroelectric materials. For example, the metal complexes [Hdabco]ReO4 (dabco = 1,4-diazabicyclo[2.2.2]octane) and $[(C_4H_9)_4N]_3Bi_2Cl_9$ have activation energies $\Delta U = 8.6$–$9.32\,\mathrm{kJ/mol}$ and $\Delta U = 11.46$–$40.60\,\mathrm{kJ/mol}$, respectively [24,56].

V. CONCLUSION

Raman spectroscopy has been used to determine the uniaxial, nonpolar order parameters of RM734. On the approach to the $\mathbf{N_F}$ phase a reduction in the uniaxial order parameter is found, and it was noted that this could be related to the reduction in the elastic constants and splay fluctuations observed by others just above the $\mathbf{N}$ to $\mathbf{N_F}$ phase transition, though other explanations have been explored here [26,27]. Throughout the $\mathbf{N}$ and $\mathbf{N_F}$ phases a reasonable agreement between $\langle P_4 \rangle$ for a given $\langle P_2 \rangle$ with predictions of the mean-field Maier-Saupe theory is found. Comparisons and differences with order parameter data determined via x ray are discussed. It is argued that Raman spectroscopy more closely agrees with Maier-Saupe predictions due to the selection of the phenyl stretching mode probing the order parameter of the rigid core of the molecule. In addition to the uniaxial order parameters, further insight may be provided about the behavior of the ferroelectric nematic phase by observing subtle changes in the Raman line width. In particular, the observed change in FWHM, Γ, of the phenyl stretching mode at the onset of the $\mathbf{N_F}$ phase is discussed. The broadening of Γ can be interpreted by analogy to solid ferroelectric materials as being a consequence of changes in the reorientational behavior of the molecules, or, the signature of the disorder-order transition from a nonpolar to a polar phase. Indeed, given that polar order is related to the ordering of the permanent dipole on the molecule, which must occur through molecular reorientation, for the $\mathbf{N_F}$ phase transition both arguments related to changes in Γ are closely related. In the framework developed for disorder-order type ferroelectric transitions, it is found that RM734 has an activation energy from paraelectric to ferroelectric of 2.5 $\pm$ 0.6 kJ/mol. While the activation energy is lower than those measured in solid ferroelectric materials [24,56], the value is of a similar order of magnitude. Therefore, it is likely that the broadening of Γ is related to the self-diffusive fluctuation of molecules from a nonpolar ordered to polar ordered state. More work is required to fully understand the temperature-dependent behavior of ferroelectric fluids via Raman spectroscopy. However, given the sensitivity of Raman spectroscopy to such behavior, it will prove useful in understanding ferroelectric behavior in polar nematic fluids.

Data sets associated with this work will be made available at Ref. [59].

ACKNOWLEDGMENTS

T.R. and H.F.G. acknowledge funding from the EPSRC, Grant No. EP/V054724/1. P.J.T. and H.F.G. acknowledge EPSRC and Merck Performance Materials Ltd. for funding through a CASE award. R.J.M. acknowledges funding from UKRI via a Future Leaders Fellowship, Grant No. MR/W006391/1, and funding from the University of Leeds via a University Academic Fellowship.

[1] M. Born, Über anisotrope flüssigkeiten. Versuch einer theorie der flüssigen kristalle und des elektrischen Kerr-effekts in flüssigkeiten, Sitzungsber Preuss Akad Wiss **30**, 614 (1916).

[2] R. J. Mandle, S. J. Cowling, and J. W. Goodby, A nematic to nematic transformation exhibited by a rod-like liquid crystal, Phys. Chem. Chem. Phys. **19**, 11429 (2017).

[3] R. J. Mandle, S. J. Cowling, and J. W. Goodby, Rational design of rod-like liquid crystals exhibiting two nematic phases, Chem. Eur. J. **23**, 14554 (2017).

[4] H. Nishikawa, K. Shiroshita, H. Higuchi, Y. Okumura, Y. Haseba, S. I. Yamamoto, K. Sago, and H. Kikuchi, A fluid liquid-crystal material with highly polar order, Adv. Mater. **29**, 1702354 (2017).

[5] A. Manabe, M. Bremer, and M. Kraska, Ferroelectric nematic phase at and below room temperature, Liq. Cryst. **48**, 1079 (2021).

[6] X. Chen, E. Korblova, D. Dong, X. Wei, R. Shao, L. Radzihovsky, M. A. Glaser, J. E. Maclennan, D. Bedrov, D. M. Walba, and N. A. Clark, First-principles experimental demonstration of ferroelectricity in a thermotropic nematic liquid crystal: Polar domains and striking electro-optics, Proc. Natl. Acad. Sci. USA **117**, 14021 (2020).

[7] N. Sebastián, L. Cmok, R. J. Mandle, M. R. de la Fuente, I. D. Olenik, M. Čopič, and A. Mertelj, Ferroelectric-ferroelastic phase transition in a nematic liquid crystal, Phys. Rev. Lett. **124**, 037801 (2020).

[8] N. Sebastián, M. Lovšin, B. Berteloot, N. Osterman, A. Petelin, R. J. Mandle, S. Aya, M. Huang, I. Drevenšek-Olenik, K. Neyts, and A. Mertelj, Polarization patterning in ferroelectric nematic liquids via flexoelectric coupling, Nat. Commun. **14**, 3029 (2023).

[9] M. van Gurp, The use of rotation matrices in the mathematical description of molecular orientations in polymers, Colloid Polym. Sci. **273**, 607 (1995).

[10] N. Sebastián, M. Čopič, and A. Mertelj, Ferroelectric nematic liquid-crystalline phases, Phys. Rev. E **106**, 021001 (2022).

[11] R. J. Mandle and A. Mertelj, Orientational order in the splay nematic ground state, Phys. Chem. Chem. Phys. **21**, 18769 (2019).

[12] B. Park, J. W. Wu, and H. Takezoe, Generalized mean-field potential description for ferroelectric ordering in nematic liquid crystals, Phys. Rev. E **63**, 021707 (2001).

[13] J. Etxebarria, C. L. Folcia, and J. Ortega, Generalization of the Maier-Saupe theory to the ferroelectric nematic phase, Liq. Cryst. **49**, 1719 (2022).

[14] R. J. Mandle, N. Sebastián, J. Martinez-Perdiguero, and A. Mertelj, On the molecular origins of the ferroelectric splay nematic phase, Nat. Commun. **12**, 4962 (2021).

[15] Z. Zhang, V. P. Panov, M. Nagaraj, R. J. Mandle, J. W. Goodby, G. R. Luckhurst, J. C. Jones, and H. F. Gleeson, Raman scattering studies of order parameters in liquid crystalline dimers exhibiting the nematic and twist-bend nematic phases, J. Mater. Chem. C **3**, 10007 (2015).

[16] Z. Zhang and H. F. Gleeson, Understanding liquid crystal order parameters deduced from different vibrations in polarised Raman spectroscopy, Liq. Cryst. **46**, 219 (2019).

[17] H. F. Gleeson, C. D. Southern, P. D. Brimicombe, J. W. Goodby, and V. Görtz, Optical measurements of orientational order in uniaxial and biaxial nematic liquid crystals, Liq. Cryst. **37**, 949 (2010).

[18] Z. Zhang, S. Kaur, B. Kundu, B. K. Sadashiva, and H. F. Gleeson, Observing the emergence of phase biaxiality in a polar smectic a system via polarised Raman spectroscopy, J. Mater. Chem. C **5**, 1195 (2017).

[19] T. Raistrick, Z. Zhang, D. Mistry, J. Mattsson, and H. F. Gleeson, Understanding the physics of the auxetic response in a liquid crystal elastomer, Phys. Rev. Res. **3**, 023191 (2021).

[20] F. Caimi, G. Nava, S. Fuschetto, L. Lucchetti, P. Paiè, R. Osellame, X. Chen, N. A. Clark, M. A. Glaser, and T. Bellini, Fluid superscreening and polarization following in confined ferroelectric nematics, Nat. Phys. **19**, 1658 (2023).

[21] K. Tashiro and M. Kobayashi, Structural phase transition in ferroelectric fluorine polymers: X-ray diffraction and infrared/Raman spectroscopic study, Phase Transit. **18**, 213 (1989).

[22] E. K. Salje, Hard mode spectroscopy: Experimental studies of structural phase transitions, Phase Transit. **37**, 83 (1992).

[23] F. Jin, L. Wang, A. Zhang, J. Ji, Y. Shi, X. Wang, R. Yu, J. Zhang, E. W. Plummer, and Q. Zhang, Raman interrogation of the ferroelectric phase transition in polar metal LiOsO3, Proc. Natl. Acad. Sci. USA **116**, 20322 (2019).

[24] Z. Zafar, A. Zafar, X. Guo, Q. Lin, and Y. Yu, Raman evolution of order–disorder phase transition in multiaxial molecular ferroelectric thin film, J. Raman Spectrosc. **50**, 1576 (2019).

[25] X. Chen, E. Korblova, M. A. Glaser, J. E. Maclennan, D. M. Walba, and N. A. Clark, Polar in-plane surface orientation of a ferroelectric nematic liquid crystal: Polar monodomains and twisted state electro-optics, Proc. Natl. Acad. Sci. USA **118**, e2104092118 (2021).

[26] A. Barthakur, J. Karcz, P. Kula, and S. Dhara, Critical splay fluctuations and colossal flexoelectric effect above the nonpolar to polar nematic phase transition, Phys. Rev. Mater. **7**, 035603 (2023).

[27] A. Mertelj, L. Cmok, N. Sebastián, R. J. Mandle, R. R. Parker, A. C. Whitwood, J. W. Goodby, and M. Čopič, Splay nematic phase, Phys. Rev. X **8**, 041025 (2018).

[28] S. Brown, E. Cruickshank, J. M. Storey, C. T. Imrie, D. Pociecha, M. Majewska, A. Makal, and E. Gorecka, Multiple polar and non-polar nematic phases, ChemPhysChem **22**, 2506 (2021).

[29] G. Durey, Polarized microscopy with the berek compensator: a comprehensive tutorial for the modern reader, Eur. Phys. J. Plus **136**, 866 (2021).

[30] W. J. Patzelt, *Polarized Light Microscopy: Principles, Instruments, Applications*, 3rd ed. (E. Leitz, Baden, 1974).

[31] W. Maier and A. Saupe, Eine einfache molekulare theorie des nematischen kristallinflüssigen zustandes, Z. Naturforsch. A **13**, 564 (1958).

[32] G. R. Luckhurst and C. Zannoni, Why is the Maier–Saupe theory of nematic liquid crystals so successful? Nature (London) **267**, 412 (1977).

[33] F. Biscarini, Z. Zannoni, C. Chiccoli, and P. Pasini, Head-tail asymmetry and ferroelectricity in uniaxial liquid crystals: model calculations, Mol. Phys. **73**, 439 (1991).

[34] A. Sanchez-Castillo, M. A. Osipov, and F. Giesselmann, Orientational order parameters in liquid crystals: A comparative study of x-ray diffraction and polarized Raman spectroscopy results, Phys. Rev. E **81**, 021707 (2010).

[35] M. T. Sims, L. C. Abbott, R. M. Richardson, J. W. Goodby, and J. N. Moore, Considerations in the determination of orientational order parameters from x-ray scattering experiments, Liq. Cryst. **46**, 11 (2019).

[36] G. Singh, J. Fu, D. M. Agra-Kooijman, J. K. Song, M. R. Vengatesan, M. Srinivasarao, M. R. Fisch, and S. Kumar,

X-ray and Raman scattering study of orientational order in nematic and heliconical nematic liquid crystals, Phys. Rev. E **94**, 060701(R) (2016).

[37] A. Sanchez-Castillo, M. A. Osipov, S. Jagiella, Z. H. Nguyen, M. Kašpar, V. Hamplová, J. MacLennan, and F. Giesselmann, Orientational order parameters of a de Vries-type ferroelectric liquid crystal obtained by polarized Raman spectroscopy and x-ray diffraction, Phys. Rev. E **85**, 061703 (2012).

[38] J. Nehring and A. Saupe, Calculation of the elastic constants of nematic liquid crystals, J. Chem. Phys. **56**, 5527 (1972).

[39] S. Kaur, J. Addis, C. Greco, A. Ferrarini, V. Görtz, J. W. Goodby, and H. F. Gleeson, Understanding the distinctive elastic constants in an oxadiazole bent-core nematic liquid crystal, Phys. Rev. E **86**, 041703 (2012).

[40] S. Kaur, H. Liu, J. Addis, C. Greco, A. Ferrarini, V. Görtz, J. W. Goodby, and H. F. Gleeson, The influence of structure on the elastic, optical and dielectric properties of nematic phases formed from bent-core molecules, J. Mater. Chem. C **1**, 6667 (2013).

[41] P. Sheng, Effect of director fluctuations on the nematic distribution function, Solid State Commun. **18**, 1165 (1976).

[42] C. Zannoni, Order parameters and orientational distributions in liquid crystals, in *Polarized Spectroscopy of Ordered Systems*, edited by B. Samorí and E. W. Thulstrup (Springer, Netherlands, 1988), pp. 57–83.

[43] N. Vaupotič, D. Pociecha, P. Rybak, J. Matraszek, M. Čepič, J. M. Wolska, and E. Gorecka, Dielectric response of a ferroelectric nematic liquid crystalline phase in thin cells, Liq. Cryst. **50**, 584 (2023).

[44] N. Kirov, I. Dozov, and M. P. Fontana, Determination of orientational correlation functions in ordered fluids: Raman scattering, J. Chem. Phys. **83**, 5267 (1985).

[45] S. Y. Yakovenko, A. A. Minko, B. Arnscheidt, and J. Pelzl, New method and results of Raman studies of non-diffusional reorientational dynamics of molecules in the nematic phase, Liq. Cryst. **19**, 449 (1995).

[46] M. P. Fontana, Raman and IR fluctuation spectroscopy of liquid crystals, in *The Molecular Dynamics of Liquid Crystals*, edited by G. R. Luckhurst and C. A. Veracini, 1st ed. (Springer, Netherlands, 1994), Vol. 1, pp. 403–428.

[47] R. Nandi, H. K. Singh, S. K. Singh, B. Singh, and R. K. Singh, Mesomorphic, micro-Raman and DFT studies of new calamitic liquid crystals; methyl 4-[4-(4-alkoxy benzoyloxy)benzylideneamino]benzoates, Spectrochim. Acta A **128**, 248 (2014).

[48] S. K. Dash, R. K. Singh, P. R. Alapati, and A. L. Verma, Dynamics of phase transitions in a liquid crystalline compound (TBDA) probed by Raman spectroscopy, J. Phys.: Condens. Matter **9**, 7809 (1997).

[49] A. Bhattacharjee, P. R. Alapati, and A. L. Verma, Dynamics of phase transitions in a liquid crystal probed by Raman spectroscopy, Liq. Cryst. **28**, 1315 (2001).

[50] N. Yadav, Y. P. Panarin, J. K. Vij, W. Jiang, and G. H. Mehl, Two mechanisms for the formation of the ferronematic phase studied by dielectric spectroscopy, J. Mol. Liq. **378**, 121570 (2023).

[51] U. Bismayer, Hard mode Raman spectroscopy and its application to ferroelastic and ferroelectric phase transitions, Phase Transit. **27**, 211 (1990).

[52] C. M. Hartwig, E. Wiener-Avnear, and S. P. S. Porto, Analysis of the temperature-dependent phonon structure in sodium nitrite by Raman spectroscopy, Phys. Rev. B **5**, 79 (1972).

[53] T. Malcherek, Displacive phase transitions, in *EMU Notes in Mineralogy: Mineral Behaviour at Extreme Conditions*, 1st ed., edited by R. Miletich (European Mineralogical Union, 2005), Vol. 7, pp. 139–171.

[54] K. M. Rabe, C. H. Ahn, and J. M. Triscone, *Physics of Ferroelectrics: A Modern Perspective*, 1st ed. (Springer, Berlin, 2007), Vol. 105.

[55] N. S. Dalal and A. Bussman-Holder, *Ferro- and Antiferroelectricity: Order/Disorder Versus Displacive* (Springer, Berlin, 2007), Vol. 124.

[56] W. Trigui and F. Hlel, Ferroelectric properties and Raman spectroscopy of the [(C4H9)4N]3Bi2Cl9 compound, RSC Adv. **9**, 24291 (2019).

[57] C. Carabatos-Nédelec and P. Becker, Order-disorder and structural phase transitions in solid-state materials by Raman scattering analysis, J. Raman Spectrosc. **28**, 663 (1997).

[58] P. da R. Andrade and S. P. S. Porto, On linewidth of phonons associated to a disorder mechanism, Solid State Commun. **13**, 1249 (1973).

[59] https://doi.org/10.5518/1491.